

# DLBFoam: An open-source dynamic load balancing model for fast reacting flow simulations in OpenFOAM

Bulut Tekgöl<sup>a,\*</sup>, Petteri Peltonen<sup>a</sup>, Heikki Kahila<sup>b</sup>, Ossi Kaario<sup>a</sup>, Ville Vuorinen<sup>a</sup>

<sup>a</sup>*Department of Mechanical Engineering, Aalto University School of Engineering, Otakaari 4, 02150 Espoo, Finland*

<sup>b</sup>*Wärtsilä Finland Oy, 65101 Vaasa, Finland*

---

## Abstract

Computational load imbalance due to direct integration of chemical kinetics is a well-known performance issue in parallel reacting flow simulations. We introduce an open-source dynamic load balancing model to address this problem within OpenFOAM, an open-source C++ library for Computational Fluid Dynamics (CFD). Due to the commonly applied operator splitting practice in reactive flow solvers, chemistry can be treated as an independent stiff ordinary differential equation (ODE) system within each computational cell. As a result of highly non-linear characteristics of chemical kinetics, a large variation in convergence rates of ODE integrator may occur, leading to a high load imbalance across multiprocessor configurations. However, the independent nature of chemistry ODE systems leads to a problem that can be parallelized easily (also termed *embarrassingly parallel* in the literature) during the flow solution. The presented model takes advantage of this feature and balances the chemistry load across available resources. When the load balancing is utilized together with a reference mapping model also introduced in this paper, a speed-up by a factor of 10 is reported for practical reactive flow simulations. To the best of our knowledge, this model is the first open-source implementation of chemistry load balancing in the literature.

**Keywords:** Reacting flows, Combustion, Load balancing, OpenFOAM, Chemical kinetics

---



---

\*Corresponding author: Bulut Tekgöl

Email address: bulut.tekgul@aalto.fi (Bulut Tekgöl)

## PROGRAM SUMMARY

*Program Title:* DLBFoam

*CPC Library link to program files:* (to be added by Technical Editor)

*Developer’s repository link:* <https://github.com/blttkg1/DLBFoam>

*Code Ocean capsule:* (to be added by Technical Editor)

*Licensing provisions:* GPLv3

*Programming language:* C++

*Supplementary material:*

*Nature of problem:* Solution of chemical kinetics in parallel reacting flow solvers raises a computational imbalance across multiprocessor architectures. DLBFoam balances the load distribution evenly, providing significant speed-up in reacting CFD applications.

*Solution method:* The dynamic load balancing is implemented by distributing the point-wise chemistry problems from most loaded processes to less loaded ones using MPI communication protocol.

*Additional comments including restrictions and unusual features:* The present model is designed to work with the standard chemistry model class available in OpenFOAM (versions 7 and 8). For the time being, the model does not support derived combustion models such as "TDAC" and covers gas-phase reaction kinetics only. In addition, the boundary surface chemistry problems are neglected by the model.

## 1. Introduction

The development of efficient Computational Fluid Dynamics (CFD) simulation tools for reacting flows is a crucial step in the research and development of less-polluting combustion concepts [1]. As the need for more detailed combustion models has become prominent, chemical kinetics models have grown in size and complexity, resulting in higher computational cost and often exceeding the computational cost of fluid dynamics by a factor of 100 [2]. Even though most CFD software utilize distributed-memory parallel architectures to their full extent, incorporating an efficient solution for reacting flows tends to lead to a high computational load imbalance during parallel execution [3].

Commonly, engineering CFD codes assume an operator-splitting strategy in reacting flow solver implementation, enabling decoupling of the chemistry and fluid dynamics in the reacting flow solution during the calculation of the chemical source terms in the governing equations [4, 5]. Therefore, changes in thermochemical composition  $\Phi$  (temperature, pressure and species concen-

trations) due to chemical reactions per computational element (e.g. finite-volume cell) are computed by solving a cell-wise independent homogeneous reaction system. The reaction system describes the rate of change of thermochemical composition as a stiff system of ordinary differential equations (ODEs), i.e.  $\partial\Phi/\partial t = f(\Phi, t)$  [4].

Typically the computational cost of the chemical source term evaluations dominates the performance metrics and creates an uneven computational load distribution in parallel applications. The difficulties occur due to the intrinsic and non-linear nature of the ODE system. As the computational cost of solving the associated stiff ODEs scales quadratically with the number of species [6], detailed reaction mechanisms easily become impractical. Furthermore, due to the vast scale separation between the fastest and slowest chemical reaction time scales, the system of ODEs is practically always numerically stiff, requiring the use of implicit time integrators with low time step values [7]. The time step value and hence the total number of floating-point operations during the integration depends on the initial thermochemical composition [8]. Furthermore, in most CFD codes parallelization is achieved with geometrical domain decomposition, leading to explicit chemistry load imbalance due to spatially and temporally varying  $\Phi$  values. A visual illustration of chemistry load imbalance is presented in Figure 1.

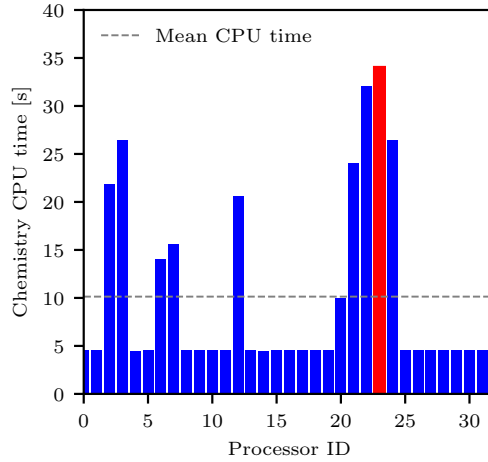


Figure 1: An illustration of the computational imbalance in a reactive CFD simulation. The cost of the chemistry solution across different processes within a given CFD time step varies, creating a bottleneck at the process with highest computational load (marked with red).

Apart from optimization of the ODE solver algorithms and implementations [6, 9, 10], several modeling strategies have been proposed to reduce the high computational requirements associated with reacting flows. To name a few successful approaches: in-situ adaptive tabulation methods [11], dynamic and adaptive reduction methods for chemical kinetics [12] and dynamic stiffness removal methods [13] each provide performance gains to certain extent. However, these strategies are often formulated in a processor-based approach, being still prone to yield computational load imbalance across available resources [14].

In the context of the present study, dynamic load balancing of chemistry has been previously covered in literature. One method to mitigate the load imbalance is to use a custom decomposition with a prior knowledge on spatial activity of chemical kinetics [15]. However, in large complex geometries, custom decomposition becomes impractical [15, 16]. In terms of dynamic run-time load-balancing algorithms, Antonelli et al. [17] developed an Message-Passing Interface (MPI) based parallel solver which utilizes a cell distribution based load balancing algorithm. Both Kodavasal et al. [18] and Shi et al. [19] considered stiffness detection approaches as balancing criteria for their balancing algorithms. Recently, Muela et al. [3] presented a dynamic load balancing method which also utilized a stiff cell detector to choose the optimal ODE integration method. In practical benchmark cases, the aforementioned methods reported speed-up factors in a range three to five.

In contrast to previous studies where implementations are either not publicly available or based on commercial CFD codes, in the present study we introduce a robust open-source load balancing algorithm for parallel reacting flow simulations. To the best of our knowledge, this model is the first open-source implementation of chemistry load balancing in literature. In addition to the load balancing model, a zonal reference mapping model is also introduced to further improve the available balancing performance. The implementation is carried out in OpenFOAM, an open-source C++ library targeted for CFD applications [20]. It is worth noting that an earlier version of this now publicly shared model has already been utilized in multiple published combustion studies by the authors [21, 22, 23].

The paper is outlined as follows: The implemented dynamic load balancing algorithm is presented in Section 2. Section 3 provides benchmarks highlighting theoretical performance gains of this model, while Section 4 reports performance metrics in practical reacting flow configurations. Section

5 concludes the study with a brief discussion on results along with potential for further improvements.

## 2. Implementation details

### 2.1. *Reacting flow solver*

A schematic of different stages of the reacting flow solver used in the paper is presented in Figure 2. Solution for mass, momentum, species and energy conservation laws is achieved in an iterative manner. The `reactingFoam` and `sprayFoam` reactive solvers of OpenFOAM [20] with compressible PIMPLE algorithm are used. Within each time step, a Poisson equation for pressure is solved and the velocities obtained from the solution of the momentum equation are corrected to ensure that mass is conserved.

Here we consider the solution of chemistry source-terms (i.e. net production/consumption rates of species concentrations) as a separate step, as highlighted in Fig. 2. In the present study, the chemistry source-terms are evaluated by direct integration of chemical kinetics with no additional models. The source-term evaluation is performed in a separate module which is interfaced from the solver level (chemistry model). The implementation of the load balancing algorithm is carried out in this module as a separate compilation unit. The details of the algorithm are discussed in the following subsection.

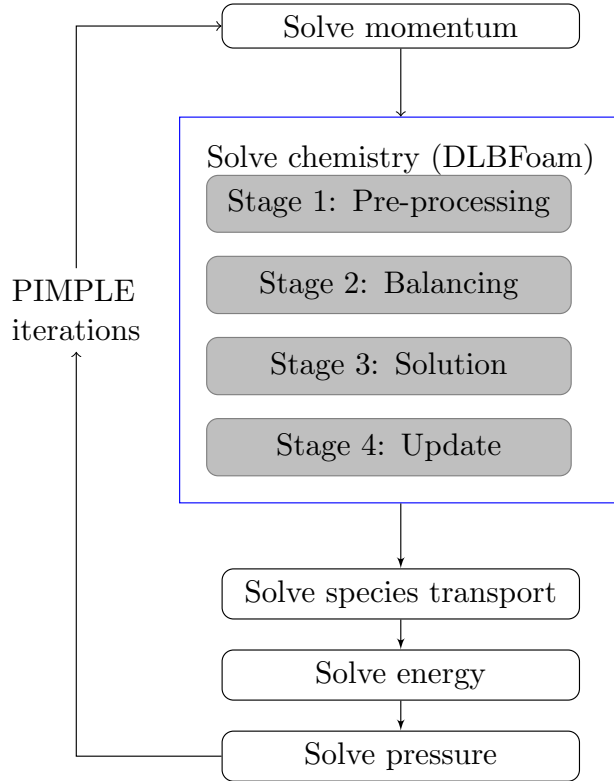


Figure 2: A schematic showing the main operations of the reactive solver in a single CFD time step. The DLBFoam is highlighted in the figure.

## 2.2. Dynamic load balancing

As mentioned before, the reaction source-term for an individual CFD cell at a certain time level can be computed independently from all the other cells. However, due to the non-linear nature of chemistry, the floating point operations required to evaluate source-terms can vary significantly from cell to cell. If the CFD domain is decomposed geometrically (as it is often done in CFD) the process with the highest chemistry load becomes the bottleneck while other processes may even idle, as illustrated in Fig. 1. The dynamic load balancing algorithm presented herein aims at redistributing the chemistry load evenly across the processes.

The dynamic load balancing implemented in the present paper consists of four stages: 1) a pre-processing stage, 2) a balancing stage 3) a solution stage and 4) an update stage. In the pre-processing stage, thermochemical variables for each cell  $n$  are packed into a single data structure, here denoted

as a **problem**, and an array of these structures is formed.

Next, an overview of stage 2 is discussed together with a pseudo-code illustration presented in Algorithm 1. The stage 2 is initiated by defining a processor-based load value  $l_k$  for all available  $N_p$  processes (line 1). Here, we define the load  $l_k$  as the sum of total CPU time spent on solving  $N_c$  problems on process  $k$ . In order to compute global balancing statistics, a sorted global list of loads  $L = [l_1, l_2, \dots, l_{N_p}]$  is formed and broadcasted to all available processes (line 2). Next, the algorithm aims at setting the global arithmetic mean load ( $\bar{L}$ ) to all processes by finding sender-receiver rank pairs  $(r_s, r_r)$  sharing a load  $\Delta L_{send}$  (line 8). Then, the CPU time based load value is converted to  $N_s$  chemistry problems to be transferred between the sender-receiver pair (line 11). Finally,  $r_s, r_r$  and  $N_s$  are inserted into a list denoted as **operations** (line 12), which is utilized to execute multiple non-blocking MPI calls to communicate the problems across processes (line 21).

In stage 3, the distributed chemistry problems are solved on their new processes. We note that the input data (a problem) is tagged with a cell id and the tag is copied to the output data (a solution) to ensure correct placement of the reaction rate in the CFD domain at the original process. In stage 4, the solutions are communicated back to the original processes based on the same  $(r_s, r_r, N_s)$  information from stage 2 and the chemical source term values of the cells are updated.

---

**Algorithm 1** Pseudo-code representation of the load balancing algorithm stage two over  $N_p$  processes w.r.t. a  $n$ th cell CPU times  $t_{\text{cpu}}^n$  at a time  $t = n+1$ .

---

```

1:  $l_k \leftarrow \sum_{n=0}^{N_c} t_{\text{cpu}}^n$  // load for rank  $k$  at given time
2:  $L \leftarrow \text{allGather}(l_k)$  // List of loads  $L = [l_1, l_2, \dots, l_{N_p}]$ 
3:  $\bar{L} \leftarrow \sum_{i=0}^{N_p} l_k / N_p$  // average load over all processes
4:  $L, R \leftarrow \text{sort}(L)$  // Sort  $L$ , and get a new rank indexing  $R$ 

5:  $i \leftarrow 0$ 
6:  $j \leftarrow N_p$ 
7: while  $i \neq j$  do
8:    $\Delta L_{\text{send}} \leftarrow \min(\bar{L} - L_i, L_j - \bar{L})$  // Define load to be transferred
9:    $r_r \leftarrow R_i$  // Rank ID receiving data
10:   $r_s \leftarrow R_j$  // Rank ID sending data
11:  find  $N_s$ , s.t.  $\Delta L_{\text{send}} \approx \sum_{n=0}^{N_s} t_{\text{cpu}}^n$  // Corresponding  $N_s$  problems
12:  operations.insert( $r_s, r_r, N_s$ ) // List of balancing operations

13:   $L_i \leftarrow L_i + \Delta L_{\text{send}}$  // Increase by the send value
14:   $L_j \leftarrow L_j - \Delta L_{\text{send}}$  // Decrease by the send value
15:  if  $|L_i - \bar{L}| \approx 0$  then
16:     $i \leftarrow i + 1$  // Move to next receiver
17:  else
18:     $j \leftarrow j - 1$  // Move to next sender
19:  end if
20: end while

21: process(operations) // Call MPI functions
22: // based on the operations list.

```

---

### 2.3. Reference mapping

In addition to the load balancing, we have implemented a reference mapping technique which allows us to further reduce the computational cost. The aim is to group cells sharing similar  $\Phi$  values together and solve chemistry only once for this group. Such a mapping approach is intended to be



used for regions with low reactivity, e.g. where no fuel is present. In our implementation, the reference mapping acts as a filter in stage 1 of the load balancing algorithm, where the reaction rate of cells satisfying certain criteria are copied from a reference cell solution. At a certain time instance, a reference cell is picked and the chemistry source term of that cell is solved and copied to other reference cells. The criteria used for identifying the reference cells is:

$$\begin{aligned} Z_i &< Z_{tol}, \\ |T_i - T_{ref}| &< T_{tol}, \end{aligned}$$

where  $Z_i$  and  $T_i$  are mixture fraction and temperature of  $i$ th cell, respectively, while  $Z_{tol}$  and  $T_{ref}$  denote user given tolerance values. In reacting flow community, mixture fraction stands for a conserved scalar describing the mixing state of a fuel and oxidizer uniquely. Although there are different definitions of  $Z$  in literature, in this paper the Bilger’s definition [24] is used. The reference solution is computed from the first reference cell found, and this solution is then mapped to the subsequent reference cells.

The reference mapping implemented in the present study is applied on each process separately. Depending on the values set of  $Z_{tol}$  and  $T_{tol}$ , as well as whether the temperature criterion is applied or not, the mapped solution and the actual solution may be slightly different from one another. As long as proper tolerances are used, the introduced error is rather small and does not affect the global characteristics of the reactive simulation. According to authors’ experience, error is negligible compared to typical uncertainties found in various combustion models. Details on validation of reference mapping against the standard model as well as a discussion on the level of error introduced is presented in [Appendix A](#).

### 3. Unit benchmarks

In this section, the performance of the load balancer model is demonstrated by using a simple test environment created in OpenFOAM. Inspired from the performance analysis presented by Muela et al. [3], we present a similar analysis to show the efficiency as well as the scaling performance of our load balancer model for: i) different number of processes and ii) different number of cells per process.

To carry out the performance analysis we have developed a benchmarking suite in OpenFOAM, where a given set of chemistry problems are solved in parallel by the ODE solver and the total execution times are measured. Two different *pseudo-problems* are pre-defined: a *heavy problem*, which is a stiff ODE problem and takes longer to compute, and a *light problem*, which is a less stiff problem with a shorter solution time. Here, a benchmark environment is created by defining the number of chemistry problems ( $N_c$ ), available resources ( $N_p$  processes) and a pre-defined  $\theta$  value, describing the ratio of *heavy problems* to number of problems in each process.

Throughout the benchmark analysis, the ratio of all the *heavy problems* to total number of problems across all processes is fixed as 0.2. Different configurations are then created to distribute the total heavy load either evenly (a balanced load configuration) or unevenly (an unbalanced load configuration). The following benchmark configurations are investigated:

- $C_1$ : "very unbalanced",  $\theta = 1$  for 20% of  $N_p$
- $C_2$ : "slightly unbalanced",  $\theta = 0.8$  for 25% of  $N_p$
- $C_3$ : "slightly balanced",  $\theta = 0.4$  for 50% of  $N_p$
- $C_4$ : "very balanced",  $\theta = 0.2$  for 100% of  $N_p$ .

The benchmark statistics are obtained by running 10 separate samples for each configuration to minimize variance due to any hardware or parallel communication issue. Each case is run first with the unbalanced (standard) model, then with the balanced model, and the speed-up ratio  $\chi_{su}$  for each condition is calculated as:

$$\chi_{su} = \frac{\tau_{unb}}{\tau_{bal}}, \quad (1)$$

where  $\tau_{unb}$  and  $\tau_{bal}$  are the mean execution times over all samples of unbalanced and balanced cases respectively.

All the simulations in this paper are carried out by the Mahti supercomputer, provided by the CSC - Finnish IT Center for Science. Mahti contains 1404 nodes with two 64 core AMD EPYC (Rome) processors each node running at 2.6 GHz, as well as high-speed 200 Gpbs infiniband HDR interconnection network between the nodes, all running on a RHEL 7.8 Linux operating system [25].

Figure 3 shows the benchmark results for configurations  $C_1$ - $C_4$  with varying  $N_p$  and  $N_c$  values. Figure 3a highlights steady performance over a large range of process counts with a fixed  $N_c = 200$ . It can be seen that the balancing algorithm scales up to  $N_p = 1280$  with no apparent performance issue. In addition, the  $\chi_{su}$  value increases with increasing imbalance ( $C_4 \rightarrow C_1$ ), since the potential balancing gain to be obtained is higher for cases with higher imbalance.

Figure 3b shows the influence of problem count  $N_c$  to balancing performance for a fixed  $N_p = 80$ . It can be clearly seen from high imbalance condition ( $C_1$ ) that the  $\chi_{su}$  first increases with increasing  $N_c$  from 40 up to 1000, then it stays in the same level for higher  $N_c$  values. The reason is two-fold: i) for lower  $N_c$  values the global mean load value ( $\bar{L}$ ) that balancer tries to reach is smaller, therefore the cost of communication is in fact comparable to the cost of gain obtained from the balancing, and ii) for lower  $N_c$  values the number of problems describing the extra load is very sensitive, e.g. the balancer may overshoot/undershoot the target load condition with a greater margin by sending one cell more/less with lower  $N_c$  values. Once the  $N_c$  value is large enough so that the communication overhead is insignificant and the number of problems that are being transferred between processes are large enough to create the balancing statistics accurately, the  $\chi_{su}$  is stabilized.

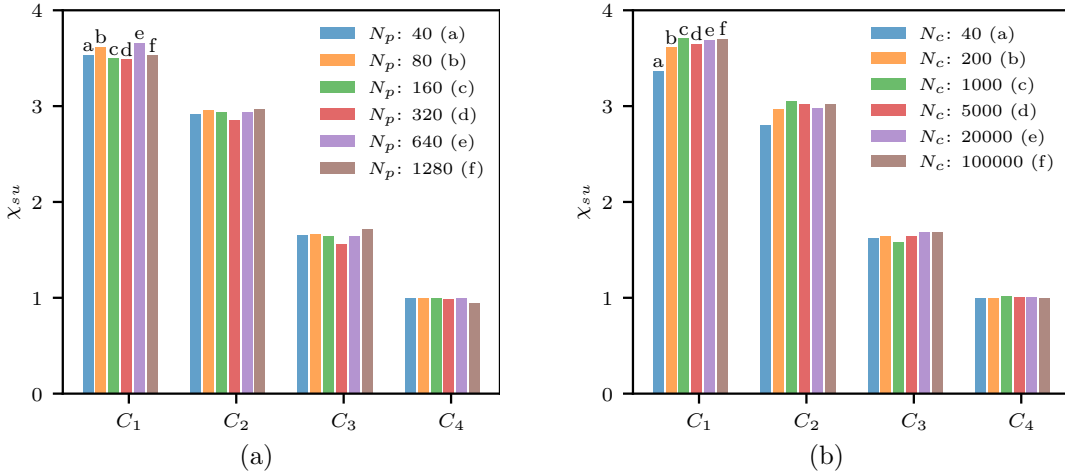


Figure 3: Speed-up ratio of a) different process counts  $N_p$  with number of problems  $N_c = 200$  b) different  $N_c$  with  $N_p = 80$ , from imbalanced ( $C_1$ ) to balanced ( $C_4$ ) configurations.

One common characteristic observed with both configurations presented in Figure 3 is the change in balancing performance with respect to the level of imbalance in the benchmark. While the increase in  $\chi_{su}$  with increased imbalance is already discussed, it is also important to note that  $\chi_{su} \approx 1$  for the very balanced case ( $C_4$ ). The  $\chi_{su}$  values close to one indicate that the operations to create the load balancing statistics to decide inter-processor communications is not resulting in significant overhead compared to ODE solution. Since the case is already perfectly balanced, the balancer does not communicate any data between the processes.

In summary, this benchmarking analysis shows that the balancing algorithm described in Section 2.2 shows very good performance and scalability for a range of process counts and chemistry problem per process values. The selected values for these two parameters are typical for reacting CFD simulations ranging from small simulations that can be run on personal computers to very large simulations that require high-performance computing clusters.

## 4. Results

Following the performance benchmark of the load balancing model in previous section, here we demonstrate the model performance in actual reactive CFD simulations. First, A 2D reactive shear layer case with a uniform mesh is simulated to show the effects of load balancing, reference mapping model, number of processes and decomposition methods. Furthermore, a 3D reactive spray LES simulation is performed to indicate a potential speed-up that can be obtained in large-scale reactive simulations. We do not present physics-based case validation, but aim to show the performance gain available with a load balancing algorithm.

### 4.1. Reactive shear layer

A schematic describing the 2D reactive shear layer configuration is presented in Figure 4. A square domain ( $8\text{mm} \times 8\text{mm}$ ) with cyclic boundary conditions is discretized by a structured mesh with  $400 \times 400$  resolution. A hyperbolic tangent function is utilized to generate a smooth shear layer of  $L/10$  width in the domain. The momentum shear layer is characterized by a relative velocity difference of  $\Delta U_x = 40\text{ m/s}$ . The shear layer instability is initiated by introducing sinusoidal perturbation for vertical velocity.

The fuel,  $n$ -dodecane ( $n\text{-C}_{12}\text{H}_{26}$ ), is placed in the middle while air ( $0.77\text{ N}_2 + 0.23\text{ O}_2$ ) is set elsewhere. The fuel and air temperatures are set to

$T_{fuel} = 400\text{ K}$  and  $T_{amb} = 900\text{ K}$ , respectively. Constant pressure of  $p = 60\text{ bar}$  is initialized in the domain. The chemical kinetics is modeled by the skeletal mechanism developed by Yao et al. [26], including 54 species and 269 reactions. The relative and absolute tolerances of the ODE solver tolerances are set to  $1e^{-5}$  and  $1e^{-8}$ , respectively. All cases are simulated over 1,000 CFD time steps with a maximum Courant number of 0.5.

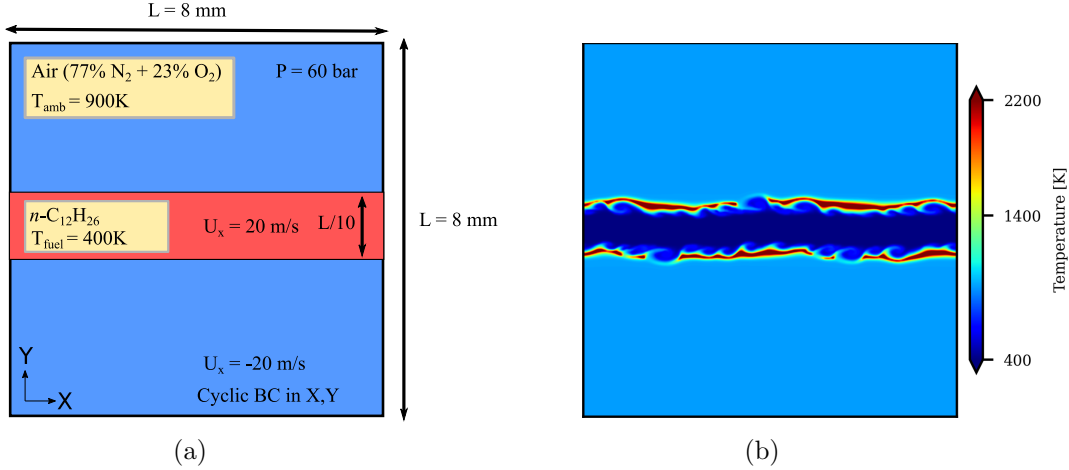


Figure 4: a) Schematic of the test case and b) an instantaneous representation of the temperature field during the simulation.

The reactivity (and the computational load) of the case is higher within the shear layer between fuel and oxidizer across X direction. Therefore this case can be decomposed using different approaches to have high or low load imbalance. Different decomposition approaches tested here are illustrated in Figure 5. While a simple decomposition in X direction (left) would ensure minimal imbalance since the decomposition is orthogonal to the shear layer, same decomposition in Y direction (middle) would result with higher imbalance since now only the processes assigned to/around shear layer will have high load, creating bottleneck. Finally, the Scotch decomposition (right) is also investigated since in many CFD applications automated and optimized decomposition methods are used to ensure uniform cell counts and minimize the process boundaries. In addition, since majority of the cells in the configuration are initially pure oxidizer (and identical), the reference mapping method can be used to significantly reduce the computational load in processes assigned to the oxidizer part, increasing the balancing performance.

Therefore, the reactive shear layer is a good test case to investigate: i) the effect of load imbalance on  $\chi_{su}$  and ii) the additional performance that can be gained from using reference mapping method together with the load balancer. The details of parameters investigated using this case (decomposition, number of processors and balancing model) are given in Table 1.

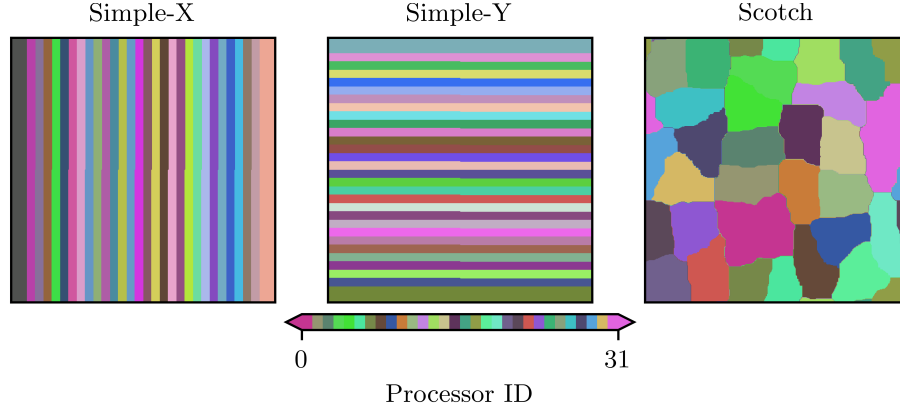


Figure 5: Decomposition of the test case to 32 processes using 1) Simple decomposition in X direction (left), 2) Simple decomposition in Y direction (middle) and 3) Scotch decomposition (right). While Simple-X attempts to reduce load imbalance, Simple-Y promotes it. Scotch decomposition by design attempts to minimize the number of process boundaries.

Table 1: The difference decomposition methods, number of processors and balancing models investigated in reactive shear layer simulations.

Decomposition	Number of processors	Models
Simple-X	32	Standard
Simple-Y	64	Loadbalanced
Scotch	128	Loadbalanced + Reference Mapping
	256	

The results obtained from the 3 different decomposition methods for  $N_p = 32$  is presented in Figure 6. It can be seen that the total execution times are significantly reduced when the load balancing is utilized. While the domain decomposition plays an important role on the performance of the standard case with no balancing, for load balanced models the execution time is not dependent on the decomposition strategy. For instance, while the Simple-Y decomposition has the highest execution time when using standard model due to load imbalance due to decomposition, the execution time of load balanced models are similar to other decomposition methods. Finally, it is important

to mention that while load balancer alone already provides substantial performance increase, utilizing the reference mapping model further increases the performance of the balancer by reducing the mean load of the simulation and creating further imbalance to increase the balancing performance.

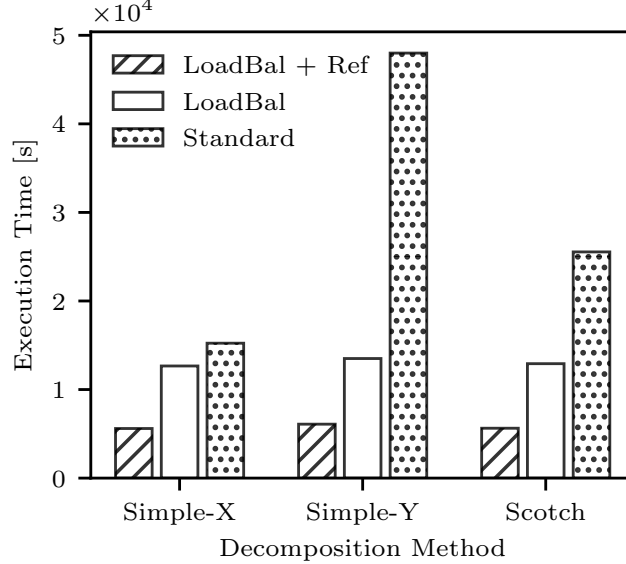


Figure 6: A bar chart showing the execution times for Simple-X, Simple-Y and Scotch decomposition methods for  $N_p = 32$ . Increase in speed-up with increased imbalance can be observed particularly from Simple-Y decomposition.

In order to further demonstrate the effect of load balancer on reactive simulations, the load, i.e. CPU time for solving the chemistry ( $\tau_{\text{cpu}}^k$ ) on each process along with its arithmetic mean across processes is presented in Figure 7 for the case with  $N_p = 32$  and Scotch decomposition. It is important to note that the profiles given here only show the time spent on solving the chemistry and does not include the time spent on balancing, which is not significant compared to  $\tau_{\text{cpu}}^k$  as shown in Section 3. It can be seen that for the non-balanced case (bottom), the deviation of  $\tau_{\text{cpu}}^k$  with respect to its mean value is very high. In this scenario, the most computationally loaded process becomes the bottleneck, while the other processes are waiting for that process to finish the chemistry computation. For load balanced cases (middle, bottom) there is very small deviation in  $\tau_{\text{cpu}}^k$  between processes with respect to the arithmetic mean, which eliminates the bottleneck caused by unbalanced chemistry load and reduces simulation time.

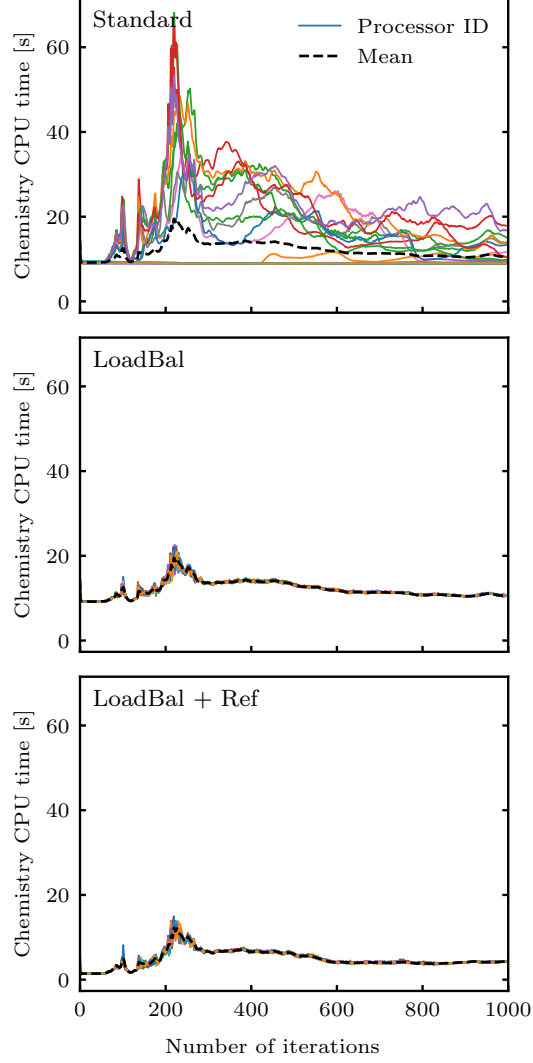


Figure 7: Chemistry solution CPU time for each process and the corresponding arithmetic mean for each configuration. It is noted that the deviation from the mean value is higher for the standard model, which causes computational performance issues.

Finally, the  $\chi_{su}$  for all cases described in Table 1 with respect to the standard model are reported in Fig. 8. For load balanced model, the  $\chi_{su}$  is small for Simple-X decomposition due to already balanced load distribution. However, for the other 2 decomposition methods a  $\chi_{su}$  around 2 to 5 can be observed. When reference mapping is also utilized, we can observe that  $\chi_{su}$  increases even further. While for Scotch decomposition  $\chi_{su} \approx 4$  to 6 is



achieved, for Simple-Y decomposition we can observe  $\chi_{su} \approx 8$  to 12.

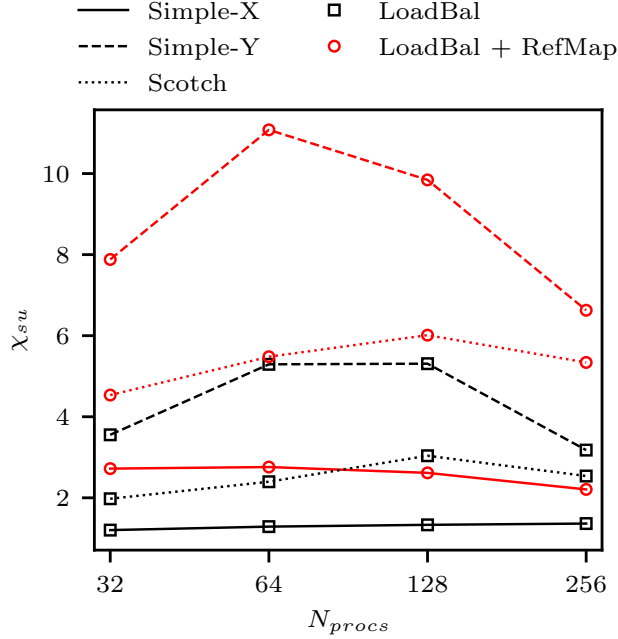


Figure 8: Speedup factor for all the cases described in Table 1. We note that the highest speedup is achieved with Simple-Y decomposition with reference mapping utilized, due to imbalance created by decomposition and balancing gain obtained by reference mapping, respectively.

#### 4.2. Three dimensional reacting diesel spray

To further demonstrate the performance of the implemented model, a larger and more challenging case is simulated in this subsection. A 3D reactive spray LES with liquid fuel injection, featuring the Engine Combustion Network Spray A condition [27] is utilized. The details of this simulation configuration can be found in our earlier work [21, 23]. A summary of the case setup is given in Table 2. A cylindrical constant volume domain with the dimensions 108x108 mm and a 1 mm base mesh along with a uniform mesh refinement region of 125  $\mu\text{m}$  enclosing the spray is used. A total of  $\approx 4.5$  M cells are decomposed into 256 processes with Scotch decomposition, resulting with  $\approx 17,000$  cells per process. A constant CFD time step of  $2e^{-7}$  s is utilized. The same chemical mechanism used in the reactive shear layer case also used here. Due to the poor performance of the standard model and our computational limitations, all simulations are started from a time

instance prior to ignition, and simulated for 500 timesteps instead of full simulations. A schematic demonstrating a portion of the computational domain is presented in Figure 9.

Table 2: Spray case setup details. See [27] for further details.

<b>ECN Spray A</b>	
Injected fuel	$n\text{-C}_{12}\text{H}_{26}$
Nominal nozzle diameter, $D$	$90\text{ }\mu\text{m}$
Injection pressure	$150\text{ MPa}$
Temperature	$900\text{ K}$
$\text{O}_2$ molar fraction	$0.15$

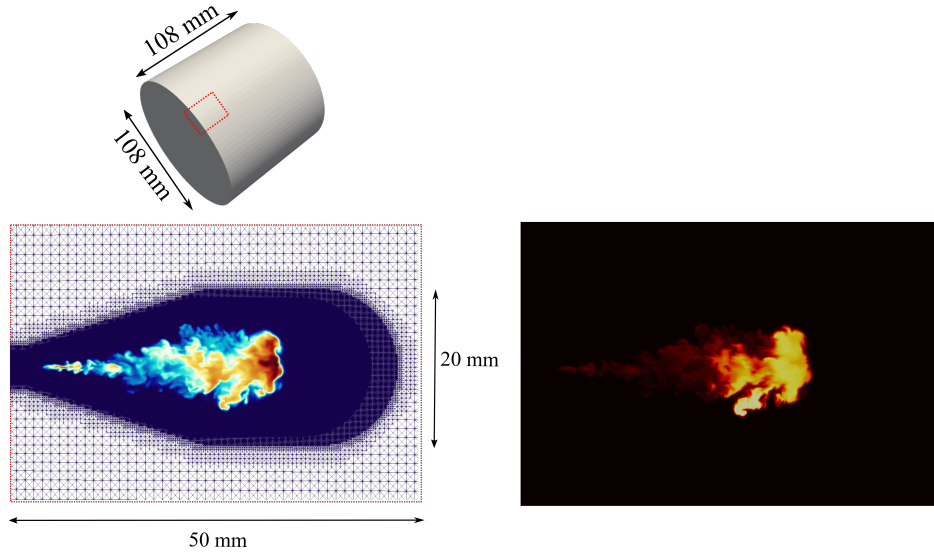


Figure 9: Schematic of the test case and the computational grid used in spray simulations based on our earlier work [21, 22, 23] (left) and an instantaneous representation of the temperature field during the simulation (right). In left figure, the mixture fraction ( $Z$ ) field is used for visualization, which gives information about the fuel mass fraction and spray vapor.

Figure 10 shows the total execution times for 3 investigated cases: standard, load balancing and load balancing with reference mapping. The computational cost of different solver operations are also timed and presented in the figure. It can be observed that the computational cost of flow equations

(momentum, pressure, energy and lagrangian) takes up a very small fraction of the total execution time. In contrast, the chemistry and the species transport equations takes up about 90 to 98 % of the total execution time. A speedup  $\chi_{su} = 2.57$  is obtained compared to the standard model when load balancing is utilized. When the reference mapping is also utilized, the  $\chi_{su}$  increases to 9.87. The gain obtained by using the reference mapping model is higher in this case compared to the reactive shear layer case presented in Section 4.1 due to the transient nature of the spray injection. The chemistry is solved within the spray region which takes up a small percentage of the total cells at the early stages of the simulation. Utilizing the reference mapping provides further speedup due to large amount of heavily idle processes outside of the spray region.

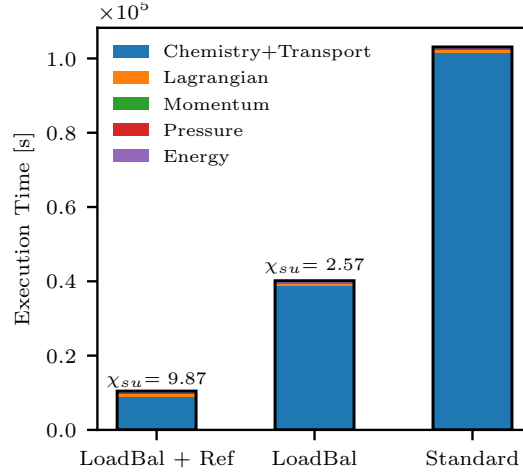


Figure 10: Speedup for different models. A speed-up by a factor of 2.57 and 9.87 obtained with load balancing and load balancing + reference mapping, respectively.

## 5. Conclusions and future work

A dynamic load balancing and a reference mapping filtering model to speed up the parallel reactive CFD simulations in OpenFOAM are presented and investigated. Dynamic load balancing utilizes MPI routines to send chemistry problems from processes with higher computational load to ones with less load, to avoid computational bottlenecks in parallel simulations. In addition, reference mapping acts as a filter, where the chemical source terms of the cells satisfying a given criteria are copied from a reference solution, instead of direct integration.

A thorough performance analysis of the model has been presented, showing its balancing efficiency to scale up to a high number of processes and number of problems per process. Furthermore, the model has been utilized on two reactive cases: a 2D reactive shear layer and a 3D diesel spray combustion case. Significant speed-up up to order of 10 to 12 has been achieved and demonstrated when load balancing and reference mapping models are used together. It is worth noting that the reported speed-up results are for the particular cases investigated, as well as the ODE solver tolerances chosen and chemical mechanism used. Changing ODE convergence tolerances and using larger/smaller chemical mechanisms may result in less or more favorable results in terms of load balancing performance.

In addition to the improvements we have introduced in this study, there are still certain aspects that can be modified to further increase the performance of the load balancing model and extend its compatibility. Two potential improvements are following:

- *Improving performance and accuracy of the ODE solvers:* Our experience on state-of-the art ODE solution algorithms including analytical Jacobian [6] and problem type tailored linear algebra [21, 10] is noted to significantly decrease ODE integrator iterations, enhance its robustness and even further increase the load-balancing efficiency.
- *Extension to in-situ tabulation and reduction models:* Presently, the implementation is not compatible with in-situ adaptive reduction and tabulation model TDAC available in OpenFOAM. Extending the load balancer to these models will both increase the load balancing performance, and mitigate the performance issues still present in TDAC due to its processor-based formulation.

Including these features to our open-source library will be investigated in the near future.

## 6. Conflict of Interest

We wish to confirm that there are no known conflicts of interest associated with this publication and there has been no significant financial support for this work that could have influenced its outcome.

## Acknowledgements

The present study has been financially supported by the Academy of Finland (grant number 318024). The computational resources for this study were provided by CSC - Finnish IT Center for Science. The first author has been financially supported by the Merenkulun Säätiö.

## Appendix A. Reference mapping model validation

The error introduced with using the reference mapping model is illustrated in Figure A.1. The figure shows the mean absolute percentage error of the volume integral of the heat release rate over all time instances relative to the results obtained with the standard chemistry model in OpenFOAM. The results are obtained from the reactive shear layer case in Section 4.1 with different process counts.  $Z_{tol} = 1e^{-4}$  and  $T_{tol} = 1$  K values are used as model tolerance. When the load balancing algorithm is used without mapping, identical results with the standard model are obtained for all process counts as expected. When the reference mapping is used a small deviation is observed as the solution slightly changing during the CFD time-integration. The deviation from the standard model depends on the process count due to the process-local nature of the reference mapping.

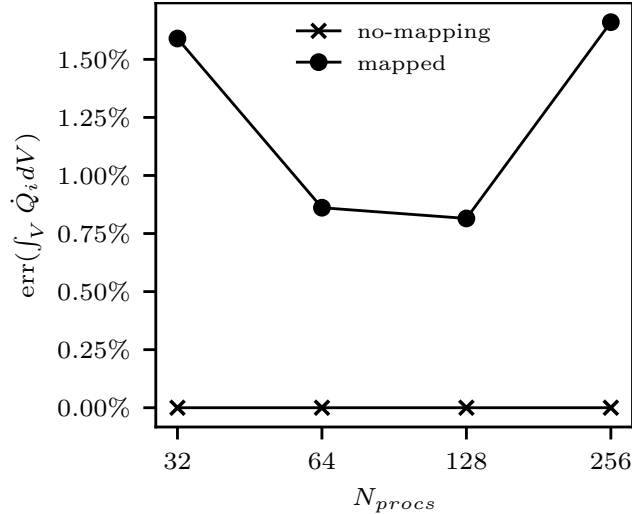


Figure A.1: The absolute percentage error of volume integrated heat release rate, averaged over all time steps.

The evolution on volume integrated heat release rate is given in Figure A.2. As seen the reference mapping shows very good match with the non-mapped models for the presented simulation data range. It is important to note that the error due to reference mapping may accumulate over time depending on the model tolerance values used. Although the performance gain when using reference mapping is significant compared to the introduced error, for applications that require very high accuracy a careful model tolerance analysis is recommended.

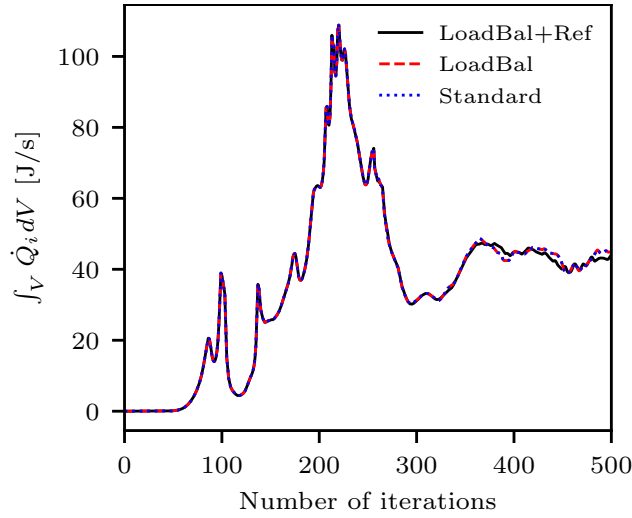


Figure A.2: Volume integrated heat release rate for  $N_p = 64$ , using load balanced + reference mapped, load balanced and standard models.

## Appendix B. Supplementary material

All the analysis in this paper is performed using the DLBFoam. DLBFoam is open-source and publicly available at <https://github.com/blttkg1/DLBFoam>. The repository contains instructions for compilation and tutorials.

## References

- [1] T. Poinso, D. Veynante, Theoretical and Numerical Combustion, Edwards, 2001.
- [2] N. Peters, Turbulent Combustion, no. 11, Cambridge University Press, Cambridge, 2000. [doi:10.1017/cbo9780511612701](https://doi.org/10.1017/cbo9780511612701).

- [3] J. Muela, R. Borrell, J. Ventosa-Molina, L. Jofre, O. Lehmkuhl, C. D. Pérez-Segarra, A dynamic load balancing method for the evaluation of chemical reaction rates in parallel combustion simulations, *Computers and Fluids* 190 (2019) 308–321. [doi:10.1016/j.compfluid.2019.06.018](https://doi.org/10.1016/j.compfluid.2019.06.018).
- [4] C. K. Law, *Combustion Physics*(Google eBook), Cambridge University Press, Cambridge, 2006. [doi:10.1017/CB09780511754517](https://doi.org/10.1017/CB09780511754517).
- [5] R. L. Speth, W. H. Green, S. MacNamara, G. Strang, Balanced splitting and rebalanced splitting, *SIAM Journal on Numerical Analysis* 51 (6) (2013) 3084–3105. [doi:10.1137/120878641](https://doi.org/10.1137/120878641).
- [6] K. E. Niemeyer, N. J. Curtis, C. J. Sung, pyJac: Analytical Jacobian generator for chemical kinetics, *Computer Physics Communications* 215 (2017) 188–203. [doi:10.1016/j.cpc.2017.02.004](https://doi.org/10.1016/j.cpc.2017.02.004).
- [7] E. Hairer, G. Wanner, *Solving ordinary differential equations. II*, Springer-Verlag, 1996. [doi:10.1007/978-3-642-05221-7](https://doi.org/10.1007/978-3-642-05221-7).
- [8] C. P. Stone, A. T. Alferman, K. E. Niemeyer, Accelerating finite-rate chemical kinetics with coprocessors: Comparing vectorization methods on GPUs, MICs, and CPUs, *Computer Physics Communications* 226 (2018) 18–29. [doi:10.1016/j.cpc.2018.01.015](https://doi.org/10.1016/j.cpc.2018.01.015).
- [9] N. Curtis, *Accelerating Reactive-Flow Simulations via Vectorized Chemical Kinetic Evaluation*, Doctoral Dissertations.
- [10] A. Imren, D. C. Haworth, On the merits of extrapolation-based stiff ODE solvers for combustion CFD, *Combustion and Flame* 174 (2016) 1–15. [doi:10.1016/j.combustflame.2016.09.018](https://doi.org/10.1016/j.combustflame.2016.09.018).
- [11] S. Pope, Computationally efficient implementation of combustion chemistry using in situ adaptive tabulation, *Combustion Theory and Modelling* 1 (1) (1997) 41–63. [doi:10.1080/713665229](https://doi.org/10.1080/713665229).
- [12] Z. Ren, Y. Liu, T. Lu, L. Lu, O. O. Oluwole, G. M. Goldin, The use of dynamic adaptive chemistry and tabulation in reactive flow simulations, *Combustion and Flame* 161 (1) (2014) 127–137. [doi:10.1016/J.COMBUSTFLAME.2013.08.018](https://doi.org/10.1016/J.COMBUSTFLAME.2013.08.018).

- [13] T. Lu, C. K. Law, C. S. Yoo, J. H. Chen, Dynamic stiffness removal for direct numerical simulations, *Combustion and Flame* 156 (8) (2009) 1542–1551. [doi:10.1016/j.combustflame.2009.02.013](https://doi.org/10.1016/j.combustflame.2009.02.013).
- [14] F. Contino, H. Jeanmart, T. Lucchini, G. D’Errico, Coupling of in situ adaptive tabulation and dynamic adaptive chemistry: An effective method for solving combustion in engine simulations, *Proceedings of the Combustion Institute* 33 (2) (2011) 3057–3064. [doi:10.1016/j.proci.2010.08.002](https://doi.org/10.1016/j.proci.2010.08.002).
- [15] H. Turkeri, X. Zhao, S. B. Pope, M. Muradoglu, Large eddy simulation/probability density function simulations of the Cambridge turbulent stratified flame series, *Combustion and Flame* 199 (2019) 24–45. [doi:10.1016/j.combustflame.2018.10.018](https://doi.org/10.1016/j.combustflame.2018.10.018).
- [16] A. Cuoci, A. Frassoldati, T. Faravelli, E. Ranzi, Numerical modeling of laminar flames with detailed kinetics based on the operator-splitting method, *Energy and Fuels* 27 (12) (2013) 7730–7753. [doi:10.1021/ef4016334](https://doi.org/10.1021/ef4016334).
- [17] L. Antonelli, P. D’Ambra, Dynamic load balancing for high-performance simulations of combustion in engine applications, in: *Proceedings - 19th International Euromicro Conference on Parallel, Distributed, and Network-Based Processing, PDP 2011*, 2011, pp. 133–140. [doi:10.1109/PDP.2011.88](https://doi.org/10.1109/PDP.2011.88).
- [18] J. Kodavasal, K. Harms, P. Srivastava, S. Som, S. Quan, K. Richards, M. Garca, Development of a Stiffness-Based Chemistry Load Balancing Scheme, and Optimization of Input/Output and Communication, to Enable Massively Parallel High-Fidelity Internal Combustion Engine Simulations, *Journal of Energy Resources Technology* 138 (5), 052203. [doi:10.1115/1.4032623](https://doi.org/10.1115/1.4032623).
- [19] Y. Shi, W. H. Green, H. W. Wong, O. O. Oluwole, Accelerating multi-dimensional combustion simulations using GPU and hybrid explicit/implicit ODE integration, *Combustion and Flame* 159 (7) (2012) 2388–2397. [doi:10.1016/j.combustflame.2012.02.016](https://doi.org/10.1016/j.combustflame.2012.02.016).
- [20] H. G. Weller, G. Tabor, H. Jasak, C. Fureby, A tensorial approach to computational continuum mechanics using object-oriented techniques, *Computers in Physics* 12 (6) (1998) 620. [doi:10.1063/1.168744](https://doi.org/10.1063/1.168744).



- [21] H. Kahila, A. Wehrfritz, O. Kaario, V. Vuorinen, Large-eddy simulation of dual-fuel ignition: Diesel spray injection into a lean methane-air mixture, *Combust. Flame* 199 (2019) 131–151. doi:[10.1016/j.combustflame.2018.10.014](https://doi.org/10.1016/j.combustflame.2018.10.014).
- [22] H. Kahila, O. Kaario, Z. Ahmad, M. Ghaderi Masouleh, B. Tekgül, M. Larmi, V. Vuorinen, A large-eddy simulation study on the influence of diesel pilot spray quantity on methane-air flame initiation, *Combustion and Flame* 206 (2019) 506–521. doi:[10.1016/J.COMBUSTFLAME.2019.05.025](https://doi.org/10.1016/J.COMBUSTFLAME.2019.05.025).
- [23] B. Tekgül, H. Kahila, O. Kaario, V. Vuorinen, Large-eddy simulation of dual-fuel spray ignition at different ambient temperatures, *Combustion and Flame* 215 (2020) 51 – 65. doi:<https://doi.org/10.1016/j.combustflame.2020.01.017>.
- [24] R. Bilger, S. Strner, R. Kee, On reduced mechanisms for methaneair combustion in nonpremixed flames, *Combustion and Flame* 80 (2) (1990) 135 – 149. doi:[https://doi.org/10.1016/0010-2180\(90\)90122-8](https://doi.org/10.1016/0010-2180(90)90122-8).
- [25] Mahti supercomputer technical specifications, <https://research.csc.fi/techspecs>, accessed: 10-09-2020.
- [26] T. Yao, Y. Pei, B. J. Zhong, S. Som, T. Lu, K. H. Luo, A compact skeletal mechanism for n-dodecane with optimized semi-global low-temperature chemistry for diesel engine simulations, *Fuel* 191 (2017) 339–349. doi:[10.1016/j.fuel.2016.11.083](https://doi.org/10.1016/j.fuel.2016.11.083).
- [27] Engine Combustion Network, Combustion Research Facility, Sandia National Laboratories, Livermore, CA, <https://ecn.sandia.gov>.